

Stability of the nonlinear dynamics of an optically injected VCSEL

J. P. Toomey,^{1,*} C. Nichkawde,¹ D. M. Kane,¹ K. Schires,² I.D. Henning,² A. Hurtado,²
and M. J. Adams²

¹ Department of Physics and Astronomy, Macquarie University, Sydney NSW 2109 Australia

² School of Computer Science and Electronic Engineering, University of Essex, CO4 3SQ, Colchester, U.K
josh.toomey@mq.edu.au

Abstract: Automated protocols have been developed to characterize time series data in terms of stability. These techniques are applied to the output power time series of an optically injected vertical cavity surface emitting laser (VCSEL) subject to varying injection strength and optical frequency detuning between master and slave lasers. Dynamic maps, generated from high resolution, computer controlled experiments, identify regions of dynamic instability in the parameter space.

©2012 Optical Society of America

OCIS codes: (250.5960) Semiconductor lasers; (250.7260) Vertical cavity surface emitting lasers; (190.3100) Instabilities and chaos.

References and links

1. S. Wieczorek, B. Krauskopf, T. B. Simpson, and D. Lenstra, "The dynamical complexity of optically injected semiconductor lasers," *Phys. Rep.* **416**(1-2), 1–128 (2005).
2. J. Ohtsubo, *Semiconductor Lasers: Stability, Instability and Chaos* (Springer-Verlag, Berlin, 2006).
3. J. Sacher, D. Baums, P. Panknin, W. Elsässer, and E. O. Göbel, "Intensity instabilities of semiconductor lasers under current modulation, external light injection, and delayed feedback," *Phys. Rev. A* **45**(3), 1893–1905 (1992).
4. E. K. Lau, L. H. Wong, and M. C. Wu, "Enhanced modulation characteristics of optical injection-locked lasers: A tutorial," *IEEE J. Sel. Top. Quantum Electron.* **15**(3), 618–633 (2009).
5. V. Annovazzi-Lodi, A. Scire, M. Sorel, and S. Donati, "Dynamic behavior and locking of a semiconductor laser subjected to external injection," *IEEE J. Quantum Electron.* **34**(12), 2350–2357 (1998).
6. T. B. Simpson, J. M. Liu, K. F. Huang, and K. Tai, "Nonlinear dynamics induced by external optical injection in semiconductor lasers," *Quantum Semiclassical Opt.* **9**(5), 765–784 (1997).
7. T. B. Simpson, "Mapping the nonlinear dynamics of a distributed feedback semiconductor laser subject to external optical injection," *Opt. Commun.* **215**(1-3), 135–151 (2003).
8. T. Perez, M. Radziunas, H. J. Wunsche, C. R. Mirasso, and F. Henneberger, "Synchronization properties of two coupled multisection semiconductor lasers emitting chaotic light," *IEEE Photon. Technol. Lett.* **18**(20), 2135–2137 (2006).
9. J. B. Altes, I. Gatare, K. Panajotov, H. Thienpont, and M. Sciamanna, "Mapping of the dynamics induced by orthogonal optical injection in vertical-cavity surface-emitting lasers," *IEEE J. Quantum Electron.* **42**(2), 198–207 (2006).
10. K. Schires, A. Hurtado, I. D. Henning, and M. J. Adams, "Comprehensive experimental analysis of nonlinear dynamics in an optically-injected semiconductor laser," *AIP Advances* **1**(3), 032131 (2011).
11. K. Schires, A. Hurtado, I. D. Henning, and M. J. Adams, "Polarization and time-resolved dynamics of a 1550-nm VCSEL subject to orthogonally polarized optical injection," *IEEE Photon. J.* **3**(3), 555–563 (2011).
12. Z. Pan, S. Jiang, M. Dagenais, R. Morgan, K. Kojima, M. Asom, R. Leibenguth, G. Guth, and M. Focht, "Optical injection induced polarization bistability in vertical-cavity surface-emitting lasers," *Appl. Phys. Lett.* **63**(22), 2999–3001 (1993).
13. I. Gatare, J. Buesa, H. Thienpont, K. Panajotov, and M. Sciamanna, "Polarization switching bistability and dynamics in vertical-cavity surface-emitting laser under orthogonal optical injection," *Opt. Quantum Electron.* **38**(4-6), 429–443 (2006).
14. K. H. Jeong, K. H. Kim, S. H. Lee, M. H. Lee, B.-S. Yoo, and K. A. Shore, "Optical injection-induced polarization switching dynamics in 1.5 μ m wavelength single-mode vertical-cavity surface-emitting lasers," *IEEE Photon. Technol. Lett.* **20**(10), 779–781 (2008).
15. A. Hurtado, I. D. Henning, and M. J. Adams, "Two-wavelength switching with a 1550 nm VCSEL under single orthogonal optical injection," *IEEE J. Sel. Top. Quantum Electron.* **14**(3), 911–917 (2008).
16. L. Chrostowski, B. Faraji, W. Hofmann, M. C. Amann, S. Wieczorek, and W. W. Chow, "40 GHz bandwidth and 64 GHz resonance frequency in injection-locked 1.55 μ m VCSELs," *IEEE J. Sel. Top. Quantum Electron.* **13**(5), 1200–1208 (2007).

17. A. Hurtado, D. Labukhin, I. D. Henning, and M. J. Adams, "Injection locking bandwidth in 1550-nm VCSELs subject to parallel and orthogonal optical injection," *IEEE J. Sel. Top. Quantum Electron.* **15**(3), 585–593 (2009).
18. I. Gatare, M. Sciamanna, M. Nizette, H. Thienpont, and K. Panajotov, "Mapping of two-polarization-mode dynamics in vertical-cavity surface-emitting lasers with optical injection," *Phys. Rev. E Stat. Nonlin. Soft Matter Phys.* **80**(2), 026218 (2009).
19. A. Hurtado, A. Quirce, A. Valle, L. Pesquera, and M. J. Adams, "Nonlinear dynamics induced by parallel and orthogonal optical injection in 1550 nm Vertical-Cavity Surface-Emitting Lasers (VCSELs)," *Opt. Express* **18**(9), 9423–9428 (2010).
20. D. M. Kane, J. P. Toomey, M. W. Lee, and K. A. Shore, "Correlation dimension signature of wideband chaos synchronization of semiconductor lasers," *Opt. Lett.* **31**(1), 20–22 (2006).
21. J. P. Toomey, D. M. Kane, M. W. Lee, and K. A. Shore, "Nonlinear dynamics of semiconductor lasers with feedback and modulation," *Opt. Express* **18**(16), 16955–16972 (2010).
22. S. Valling, T. Fordell, and A. M. Lindberg, "Experimental and numerical intensity time series of an optically injected solid state laser," *Opt. Commun.* **254**(4-6), 282–289 (2005).
23. S. Valling, T. Fordell, and A. M. Lindberg, "Maps of the dynamics of an optically injected solid-state laser," *Phys. Rev. A* **72**(3), 033810 (2005).
24. S. Valling, B. Krauskopf, T. Fordell, and A. M. Lindberg, "Experimental bifurcation diagram of a solid state laser with optical injection," *Opt. Commun.* **271**(2), 532–542 (2007).
25. J. P. Toomey, D. M. Kane, S. Valling, and A. M. Lindberg, "Automated correlation dimension analysis of optically injected solid state lasers," *Opt. Express* **17**(9), 7592–7608 (2009).
26. F. Koyama, "Recent advances of VCSEL photonics," *J. Lightwave Technol.* **24**(12), 4502–4513 (2006).
27. A. Argyris, D. Syvridis, L. Larger, V. Annovazzi-Lodi, P. Colet, I. Fischer, J. García-Ojalvo, C. R. Mirasso, L. Pesquera, and K. A. Shore, "Chaos-based communications at high bit rates using commercial fibre-optic links," *Nature* **437**(7066), 343–346 (2005).
28. J. S. Lawrence and D. M. Kane, "Nonlinear dynamics of a laser diode with optical feedback systems subject to modulation," *IEEE J. Quantum Electron.* **38**(2), 185–192 (2002).
29. S. Eriksson and A. M. Lindberg, "Observations on the dynamics of semiconductor lasers subjected to external optical injection," *J. Opt. B.* **4**(2), 149–154 (2002).
30. S. Eriksson and A. M. Lindberg, "Periodic oscillation within the chaotic region in a semiconductor laser subjected to external optical injection," *Opt. Lett.* **26**(3), 142–144 (2001).
31. T. Fordell and A. M. Lindberg, "Numerical stability maps of an optically injected semiconductor laser," *Opt. Commun.* **242**(4-6), 613–622 (2004).
32. C. Bonatto and J. A. C. Gallas, "Accumulation horizons and period adding in optically injected semiconductor lasers," *Phys. Rev. E Stat. Nonlin. Soft Matter Phys.* **75**(5), 055204 (2007).
33. V. Kovanis, A. Gavrielides, and J. A. C. Gallas, "Labyrinth bifurcations in optically injected diode lasers," *Eur. Phys. J. D* **58**(2), 181–186 (2010).
34. M.-R. Park, O.-K. Kwon, W.-S. Han, K.-H. Lee, S.-J. Park, and B.-S. Yoo, "All-monolithic 1.55 μm InAlGaAs/InP vertical cavity surface emitting lasers grown by metal organic chemical vapor deposition," *Jpn. J. Appl. Phys.* **45**(1), L8–L10 (2006).
35. M. Sciamanna and K. Panajotov, "Two-mode injection locking in vertical-cavity surface-emitting lasers," *Opt. Lett.* **30**(21), 2903–2905 (2005).
36. K. Schires, A. Hurtado, I. D. Henning, and M. J. Adams, "Analysis and characterisation of experimental real-time series of a semiconductor laser under optical injection," in *Conference on Lasers and Electro-Optics Europe and 12th European Quantum Electronics Conference (CLEO EUROPE/EQEC)* (Munich, Germany, 2011).
37. S. Wieczorek, B. Krauskopf, and D. Lenstra, "Multipulse excitability in a semiconductor laser with optical injection," *Phys. Rev. Lett.* **88**(6), 063901 (2002).
38. B. Krauskopf, K. Schneider, J. Sieber, S. Wieczorek, and M. Wolfrum, "Excitability and self-pulsations near homoclinic bifurcations in semiconductor laser systems," *Opt. Commun.* **215**(4-6), 367–379 (2003).
39. L. Olejniczak, K. Panajotov, H. Thienpont, and M. Sciamanna, "Self-pulsations and excitability in optically injected quantum-dot lasers: Impact of the excited states and spontaneous emission noise," *Phys. Rev. A* **82**(2), 023807 (2010).
40. B. Kelleher, C. Bonatto, G. Huyet, and S. P. Hegarty, "Excitability in optically injected semiconductor lasers: contrasting quantum-well- and quantum-dot-based devices," *Phys. Rev. E* **83**(2), 026207 (2011).
41. D. M. Kane and J. P. Toomey, "Variable pulse repetition frequency output from an optically injected solid state laser," *Opt. Express* **19**(5), 4692–4702 (2011).
42. K. Petermann, *Laser Diode Modulation and Noise* (Kluwer Academic Publishers, Dordrecht, 1988).

1. Introduction

The dynamics of semiconductor lasers are known to be quite susceptible to external influences, such as optical feedback, modulation or injection [1–3]. In particular, optical injection has been shown to provide enhanced modulation bandwidth [4] as well as a variety of nonlinear dynamics. The latter range from periodic oscillatory output to chaotic behavior [5,6]. The complex nonlinear dynamics arising from optical injection have been investigated using a variety of semiconductor lasers, including edge-emitting Fabry Perot [6], distributed

feedback (DFB) [7], multi-section [8] and vertical cavity surface emitting laser (VCSEL) devices [9–19].

Typically, studies of the complex phenomena in these systems have used electrical and optical frequency spectral measurements of the output from the lasers to characterize and analyze the dynamics. The recent availability of fast optical detectors and high bandwidth real-time oscilloscopes means that temporal information, unavailable to earlier studies, can now be readily accessed. Investigations on experimental laser intensity time series have been reported on edge-emitting semiconductor lasers with optical feedback [20] and injection current modulation [21], optically injected solid state lasers [22–25] and optically injected VCSELs [10, 11].

VCSEL devices have a number of practical, beneficial features relative to other semiconductor lasers such as on-wafer testing capabilities, reduced manufacturing costs, high coupling efficiency to optical fibers, ease of integration into 2D arrays and low threshold currents [26]. For these reasons, combined with the potential for nonlinear laser outputs to be used in applications such as secure optical data communication [27], nonlinear dynamics from VCSEL systems has current priority in nonlinear laser studies. A number of optical injection VCSEL based system investigations have been reported. These have looked at the interesting dynamics resulting from polarized optical injection of VCSELs. The light from a master laser is injected into one of the two orthogonally polarized modes associated with the fundamental transverse mode of the slave laser. In general, the current through the free running VCSELs can be set so that only one of the polarized modes is lasing. Orthogonal injection is where the injected master laser light is polarized orthogonally to that of the free running slave laser emission. Similarly, parallel injection is where the injected light has the same polarization as the free running mode of the slave laser. A variety of phenomena has been observed including polarization switching and polarization bistability in short wavelength (approx. 835-845 nm) [12, 13], and long wavelength (approx. 1.5 μm) VCSELs [14, 15], injection locking [16, 17], nonlinear dynamics and chaos [10, 11, 18, 19].

The majority of studies on optically injected VCSELs look at the system dynamics whilst varying the injected polarization, injection strength and the frequency detuning between the injected mode and the free running slave laser mode. Dynamic maps of the experimental laser output, categorized into the basically different types of output observed, are an effective way of displaying different regions of operation within the parameter space. Such maps have previously been generated for an 845 nm VCSEL subject to orthogonally polarized injection [9], and a 1550 nm VCSEL with both parallel and orthogonal polarized injection [19].

Similar maps have been produced for semiconductor lasers with optical feedback and modulation [28] and optically injected edge emitting semiconductor lasers [29]. Careful experiments have uncovered regions of periodic output embedded in otherwise chaotic regions [29,30]; a feature that is also present in theoretical models of the system [31–33]. These results show the need to explore the parameter space at high resolution with respect to changes in the drivers of the nonlinear dynamics. These drivers are injection strength and frequency offset in the case of optical injection [29–33].

One aspect of the injected VCSEL systems that has not been addressed is the stability of the dynamics for fixed parameter settings. The notion of stability as used in the context of this work is one by which the system produces basically the same type of dynamics, a type of stationarity, over time for a single operation condition of the system. In some cases the dynamic state may be observed to be unstable in time and it is in such situations that we are referring to an ‘instability of the instability’. Most applications would require a system to continuously produce the same type of dynamics once set in a particular mode of operation. In this work we report on the polarization resolved nonlinear dynamics and stability of a 1550 nm VCSEL subject to orthogonally-polarized optical injection. We present maps highlighting regions of operation where the dynamics are unstable and nonstationary, despite having fixed system parameters. The instabilities observed in the nonlinear dynamics for a given set of parameters are found to be richer for optical injection by an orthogonally polarized light into

the orthogonal mode of the slave laser. For this reason, this case is the one mostly reported and discussed in this paper.

2. Experimental setup

The experimental arrangement is the same as that described in [11]. The main features are reproduced here in Fig. 1.

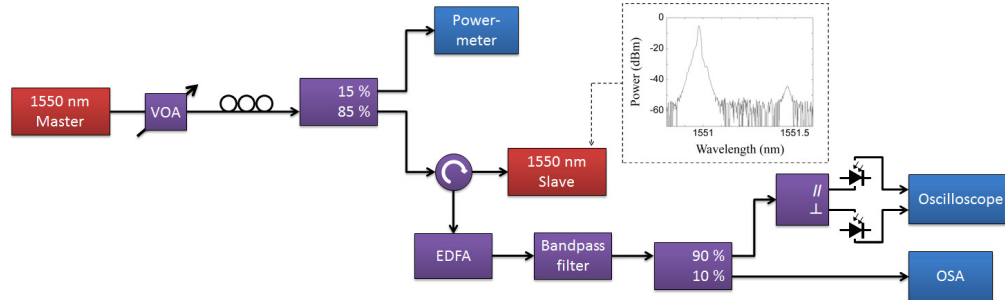


Fig. 1. Setup used for the study of orthogonally polarized injection in a 1550 nm VCSEL (reproduced from [11]).

An external cavity master laser with tunable optical frequency provided the external injection for the 1550 nm slave VCSEL. The slave laser was a commercially available InAlGaAs/InP QW 1550 nm VCSEL [34]. A polarization controller adjusted the master laser polarization to be orthogonal relative to the free-running VCSELs lasing mode. The injection strength was controlled using a variable optical attenuator. A coupler sent 15% of the master laser output power to a power meter to monitor the injection strength. The remaining 85% was sent to the slave VCSEL via an optical circulator. The VCSEL emission was separated using the circulator and amplified by an erbium-doped fiber amplifier (EDFA). The broadband amplified spontaneous emission (ASE) noise from the EDFA was removed from the signal prior to analysis using a bandpass filter centered on the VCSEL wavelength. The output power from the slave laser was resolved into components with parallel and orthogonal polarization using a polarization beam splitter. Both polarizations were monitored simultaneously using closely matched 12 GHz photodiodes on separate channels of a 13 GHz real-time oscilloscope (Agilent DSA91304A) which recorded time series of 100 ns in length (32 017 data points). Additionally some of the output signal was also sent to an optical spectrum analyzer (OSA) to monitor the spectral characteristics.

The slave laser relaxation oscillation frequency is approximately 4 GHz. Threshold current was 1.8 mA at 293 K. The device exhibits two modes that correspond to the orthogonal polarizations of the fundamental transverse mode. The device operated on a single transverse mode under all conditions in this work. The optical spectrum inset in Fig. 1 shows the main lasing mode (at -5 dBm) and subsidiary mode (at -44 dBm) separated by approximately 0.5 nm (60 GHz) in the free running slave laser output. Throughout the remainder of this paper the main lasing mode will be referred to as the parallel polarization and the subsidiary mode as the orthogonal polarization.

Both parallel and orthogonal polarization intensity time series were recorded at 2021 different parameter combinations of injection strength (K) and frequency detuning (Δf). Injection strength is defined as the power in the injection channel normalized to the power of the free running VCSEL. Frequency detuning is the difference between the center optical frequency of the injected mode and the center frequency of the orthogonally polarized mode of the slave VCSEL. In this work the parameter range of interest covers injection strengths from approximately -15 dB up to $+7.2$ dB and frequency detuning from -10.9 GHz to $+13.1$ GHz. The frequency detuning was limited to this range as no interesting dynamics were observed outside of these limits for the maximum amount to power able to be injected into the VCSEL. It has been reported by Sciamanna et al. [35] that different dynamical scenarios can

be expected as the detuning approaches the frequency separation between the polarization modes. In this case, the device mode separation (~ 60 GHz) is quite large. An investigation into the dynamics of devices subject to frequency detuning values comparable with the polarization mode separation is the subject of future work.

3. Results and discussion

3.1 Dynamic maps

The majority of the results presented here are based on the orthogonally polarized time series. It is injected light of this polarization which results in the dominant output mode of the slave laser having orthogonal polarization, and which leads to dynamical outputs which show the most cases of changing in time within the mapped parameter regions. Unless it is explicitly stated otherwise, the reader should assume the results are for the orthogonal polarization.

This data has been analyzed previously and maps have been manually generated which show the boundaries between the different dynamic regions, including stable injection locking (SIL), limit cycle or period-1 (P1), period doubling (P2) and chaos (C) [36].

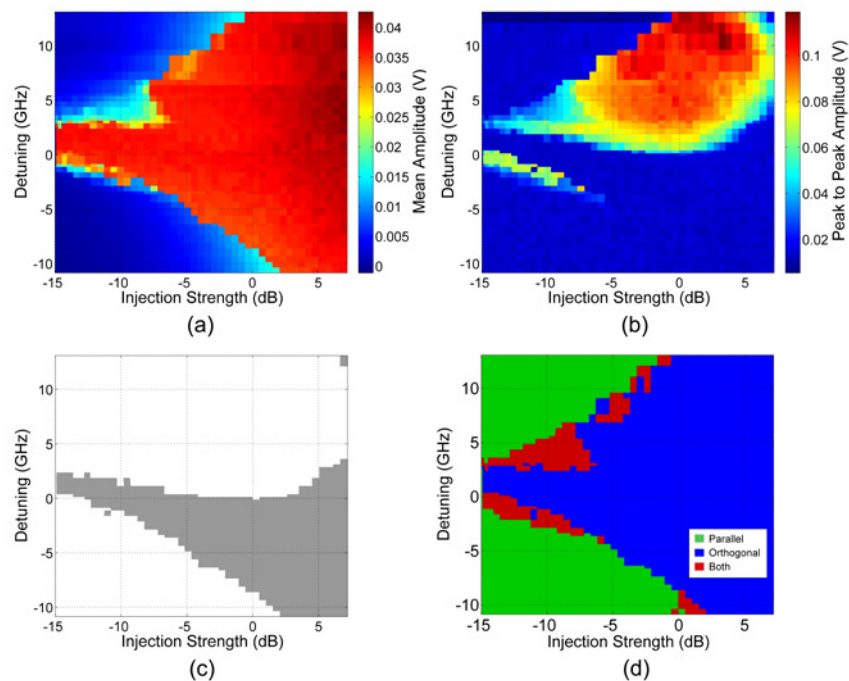


Fig. 2. Maps of the orthogonal polarization (a) average amplitude and (b) peak-to-peak amplitude when combined can produce a map of the (c) stable injection locked region, (d) identifies regions that display one or two polarization mode operation.

In this work, automated algorithms were produced to determine various measurements from the time series. Average intensity (Fig. 2(a)) and peak-to-peak amplitude (Fig. 2(b)) measurements were used to determine parameters where the laser is injection locked. Time series with high mean intensity and low peak-to-peak amplitude are representative of a stable injection locked output. The maps in Fig. 2 summarize these measurements and the resulting stable injection locked region is shown in Fig. 2(c). The map in Fig. 1(d) represents the regions where the slave VCSEL is operating on the parallel polarization only, the orthogonal polarization only, or both. This is determined by checking if the amplitude exceeds the noise threshold (set at 20 mV) at any point during the time series.

Outside of the injection locked region a variety of dynamics can be observed. In most cases the dynamics remain constant, or stationary, while held at a fixed detuning and injection

strength. See Fig. 3 for typical time series from the positive frequency detuning region showing period-1 (P1) and period doubling (P2) dynamics.

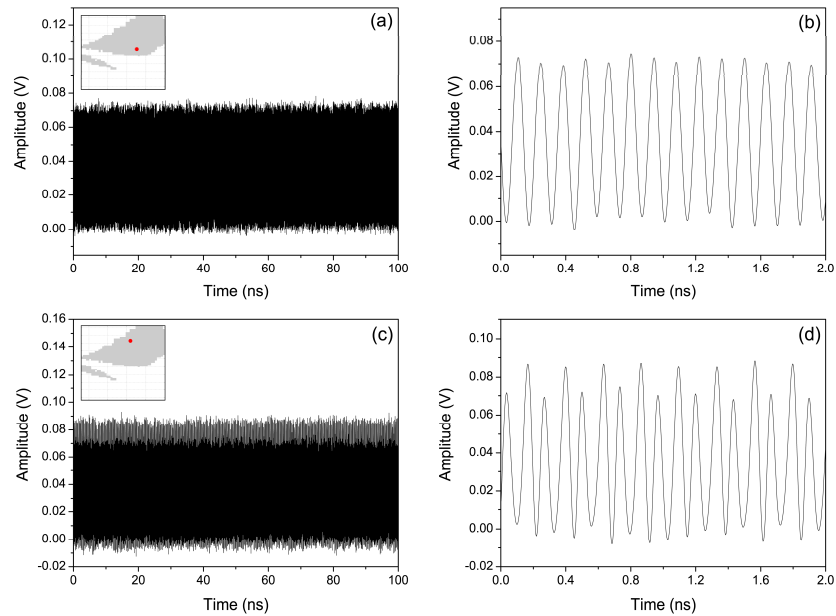


Fig. 3. Orthogonal polarization intensity time series remaining stationary over the 100 ns trace. (a) P1 ($K = -0.55$ dB, $\Delta f = +2.37$ GHz) and (c) P2 ($K = -2.15$ dB, $\Delta f = +9.10$ GHz). Plots in (b) and (d) are the same graphs on a much shorter time scale. The inset maps show the location of the particular time series in the parameter space. For clarity, grey regions are included in the inset maps which represent dynamics with peak-to-peak-amplitudes greater than 0.02 V.

In these stationary regions the dynamics remain constant for the duration of the 100 ns time series. Under these conditions, the optically injected VCSEL system could have applications as a periodic signal source.

3.2 Dynamic instabilities/nonstationarity

Within the parameter space large regions of stationary dynamics were observed, however we also observed nonstationarities within the 100ns traces in some regions particularly near region boundaries between two attractors. Great care was taken to ensure measurements were conducted under stable conditions and while we cannot rule out extreme sensitivity to experimental conditions, these features are believed to be of a fundamental nature. Some examples of the types of observed unstable dynamics are shown in Fig. 4.

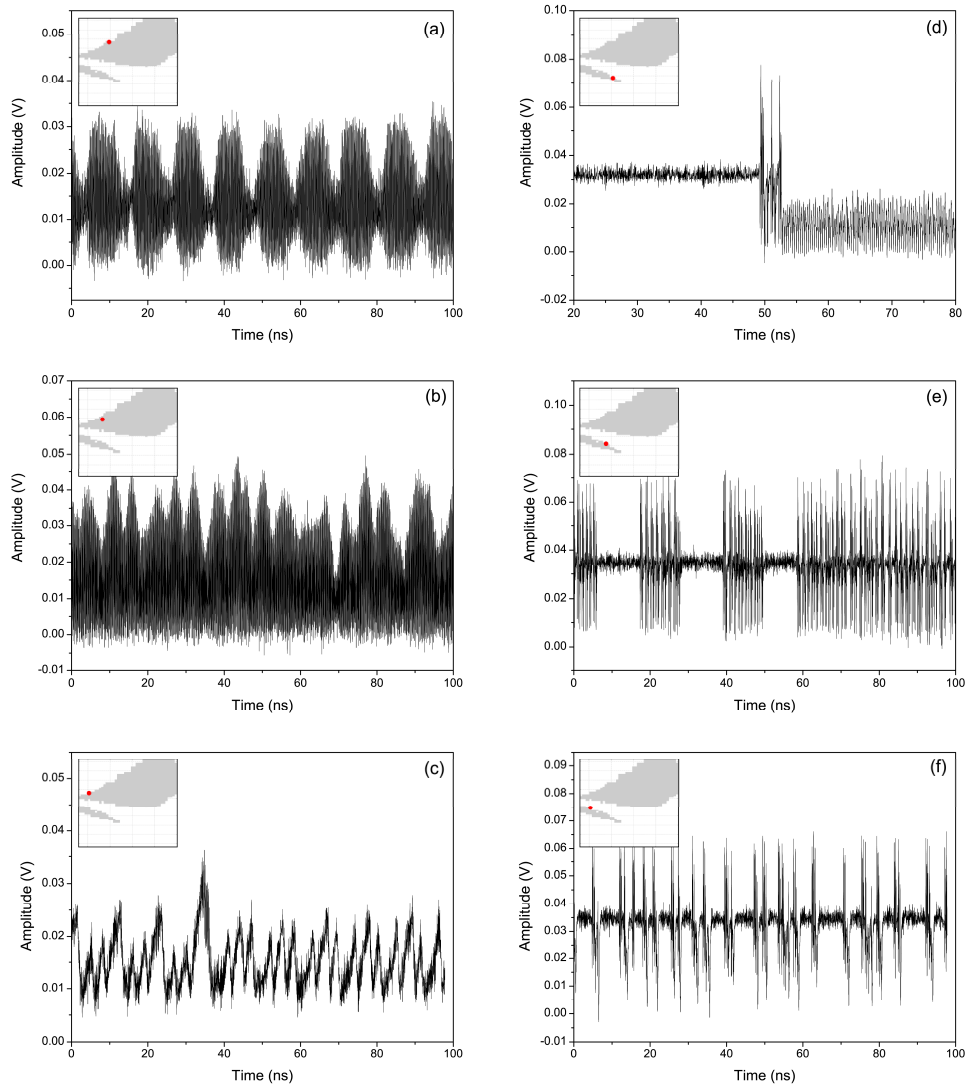


Fig. 4. Some of the various dynamics (orthogonal polarization) that can be detected using this method; (a) $\Delta f = +4.86$ GHz, $K = -9.83$ dB, (b) $\Delta f = +6.86$ GHz, $K = -8.37$ dB, (c) $\Delta f = +4.36$ GHz, $K = -12.84$ dB, (d) $\Delta f = -2.87$ GHz, $K = -7.74$ dB, (e) $\Delta f = -1.62$ GHz, $K = -9.27$ dB, (f) $\Delta f = -0.87$ GHz, $K = -12.74$ dB. The inset maps show the location of the particular time series in the parameter space. For clarity, grey regions are included in the inset maps which represent dynamics with peak-to-peak-amplitudes greater than 0.02 V.

The different time-series displayed in Fig. 4 are representative of the types of dynamics detected by the techniques described later in Section 3.3. The examples in Figs. 4(a)-4(c) are typical of the dynamics seen at positive frequency detuning. These types of dynamics are similar to those seen in various complex nonlinear systems and, although they appear quite irregular, do not seem to be switching between different dynamic states. In Fig. 4(a) a high frequency periodic oscillation is modulated by a much lower frequency envelope, much like a noisy amplitude modulation (AM). The time series in Fig. 4(b) is similar to that seen in Fig. 4(a); i.e. a high frequency periodic oscillation, only this time with a chaotically varying amplitude modulation. Low amplitude, low frequency fluctuations, such as those seen in Fig. 4(e), are typically observed for positive frequency detuning and low injection strengths.

In contrast, the time-series in Figs. 4(d)-4(f) represent much more dramatic switching between what appear to be different dynamic states. These can be seen for negative frequency detuning values. Figure 4(d) shows a rapid switch from stable injection locked output to noisy P1 dynamics. The transition period between the two states consists of several spikes in the laser intensity. A switching between injection-locked output and chaotic pulsing is observed in Fig. 4(e). A spiky output can be seen in Fig. 4(f) which is from a similar parameter space as Fig. 4(e). This type of dynamic shows strong similarities with the excitability pulses reported theoretically [37–39] and experimentally [40] in edge-emitting semiconductor lasers.

If this optically injected VCSEL system is to be utilized as a source of periodic or chaotic signals then these regions where significant variations in the dynamics occur need to be identified and avoided.

3.3 Detecting unstable dynamics: amplitude variations

A technique is implemented in which a sliding window of 200 points (approx. 625 ps) is passed over the 32 017 point (100 ns) normalized time series. The peak-to-peak amplitude of the normalized time series within each of the 160 windows is recorded and the standard deviation is used to identify time series that show unstable dynamics. The size of the window used can be adjusted to look for variations on different time scales. The sub-nanosecond window used here results in the identification of time-series which may be stationary over longer time scales, such as those previously shown in Figs. 4(a)-4(c).

Data sets with a peak-to-peak amplitude standard deviation of greater than a certain threshold are flagged as having a significant change in dynamics. A map of the standard deviation for the orthogonal polarization is shown in Fig. 5(a), and for the parallel polarization in Fig. 5(b).

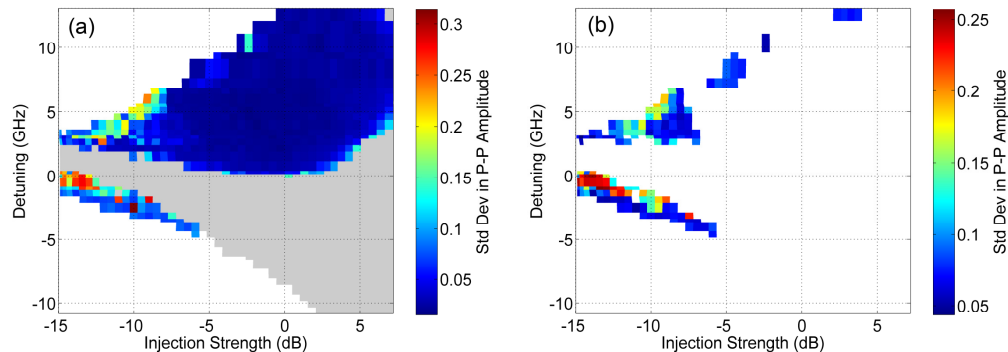


Fig. 5. Maps of the windowed peak to peak amplitude standard deviation for (a) orthogonal, and (b) parallel polarization. The grey region represents injection locked dynamics.

For both polarizations, a standard deviation above 0.05 was determined to be indicative of time series with changing dynamics. Using this threshold, a simplified map is shown in Fig. 6 which depicts the regions where either the orthogonal, parallel, or both polarizations are unstable.

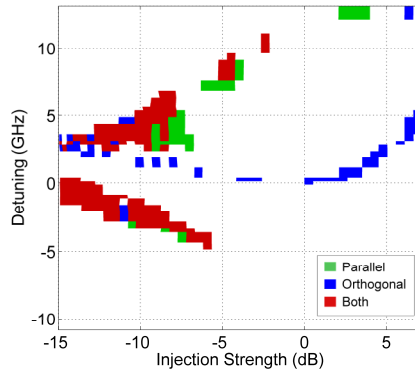


Fig. 6. Map showing the regions where the unstable nonstationary dynamics occur in parallel polarization only (red), orthogonal polarization only (green) and both polarizations (blue).

The ‘unstable’, or nonstationary, points are generally located in a region extending from $\Delta f = 0$ GHz, $K = -15$ dB to $\Delta f = -4.9$ GHz, $K = -6$ dB, and also along the boundaries of the high peak amplitude region for positive frequency detuning.

Many of the time series identified in the parallel polarization data set as having variable dynamics are for the same parameter settings as the orthogonal map. These points are colored red in Fig. 6. In these regions of the parameter space, strong correlations (or anti-correlations) between the parallel and orthogonal polarizations mean that nonstationary dynamics seen in one polarization are replicated in the other. An example of this anti-correlation between the polarizations is shown in Fig. 7.

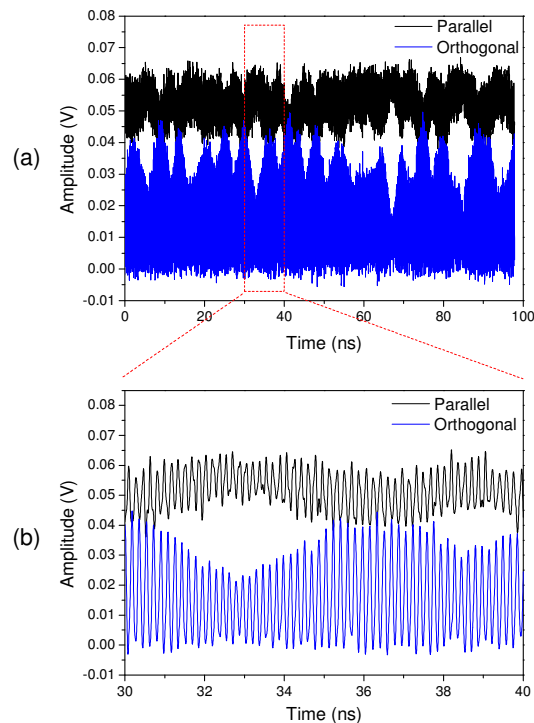


Fig. 7. (a) Time series of both orthogonal and parallel polarizations for $\Delta f = +6.86$ GHz, $K = -8.37$ dB. (b) Expanded region showing the polarization switching (note that the parallel trace has been shifted by 2.18 ns so that the two time series are synchronized. This corrects for delays due to distances to detector and electrical components. Also, the amplitude of the parallel trace has been offset by +0.03 V for clarity).

The maps showing the nonstationary regions of the parameter space in Figs. 5 and 6 are based on variations in the amplitude of the intensity time series. Another way to identify regions of changing dynamics is to look at temporal variations.

3.4 Detecting unstable dynamics: temporal variations

Previous study of an optically injected solid-state laser led to the development of a technique to measure ‘timing jitter’ in experimental intensity time series [41]. The method involves measuring the standard deviation of the period between consecutive local maxima in the time series. Any time series with a significant standard deviation, as a percentage of the mean period, is likely to display varying, nonstationary dynamics. The process of locating the local maxima in the time series meant the dominant frequency of the dynamics could also be determined at the same time by calculating the average period between them.

The maps in Figs. 8(a) and 8(b) represent the standard deviation of the time period between local maxima, as a percentage of the average period, and the dominant frequency of the time series, respectively. Note that the analysis was restricted to time series which have peak-to-peak amplitude greater than 20 mV so as to remove the time series which show low amplitude noise.

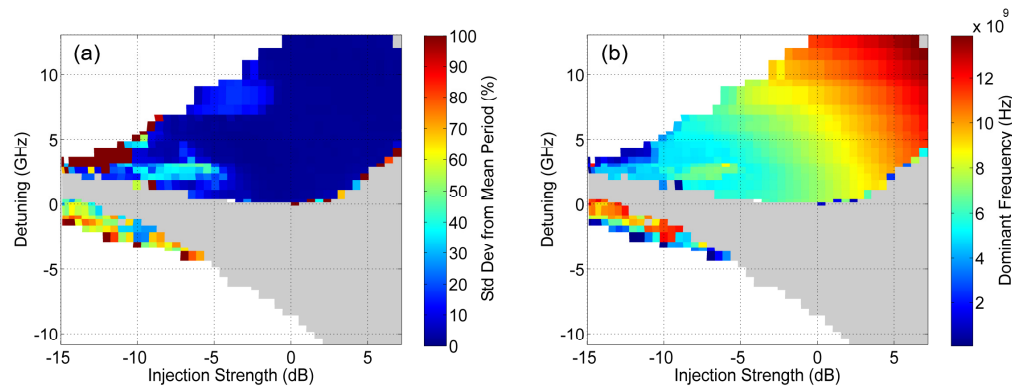


Fig. 8. (a) Map of the standard deviation in time interval between local maxima as a percentage of the average time interval, and (b) map of the dominant frequency as determined by the average time interval (period) between local maxima. The grey region represents injection locked dynamics.

This gives a measure of temporal stability in the dynamics by mapping the variation in the time interval between local maxima. The grey and clear regions of the maps in Fig. 8 have small peak-to-peak amplitude (< 20 mV) and are identified as having no ‘interesting’ dynamics, i.e. when the laser is injection locked (grey region) or the power is predominantly emitted in the parallel polarization mode (clear region).

The regions identified in Fig. 8(a) as having a significantly large standard deviation from the mean time interval, generally match the areas in the amplitude-variation map (Fig. 6), identified as being nonstationary. The average time interval between maxima can be interpreted as a period in most cases where the standard deviation is low. This period was used to generate the frequency map in Fig. 8(b).

There are noticeable differences between the unstable dynamics seen in the isolated region for negative frequency detuning to those seen on the boundary of the stable region for positive frequency detuning.

3.5 Positive frequency detuning

For positive frequency detuning values, the area of ‘interesting’ dynamics, as highlighted in Fig. 8, is bounded by the injection locked region below and a region of noisy, low amplitude dynamics above (when the device is lasing predominantly on the parallel polarization mode).

Increasing injection strength causes a transition from the injection locked region to the stable region for detuning values 0 GHz to 2.37 GHz. This transition is observed as a P1 oscillation with gradually increasing amplitude.

The transition from the low power region into the stable region (detuning values ≥ 2.87 GHz) varies depending on the magnitude of the detuning. From the data captured in this experiment, several distinct transitions were identified.

In the range of 2.87 GHz to 4.86 GHz, increasing injection strength causes the dynamics to transition from a low power, noisy output to stable P1 via a low frequency fluctuation state, where the two polarizations compete, followed by a noisy P1 state. As injection strength was increased the noisy periodic oscillation increased in amplitude to become clean P1 dynamics as seen in Fig. 9.

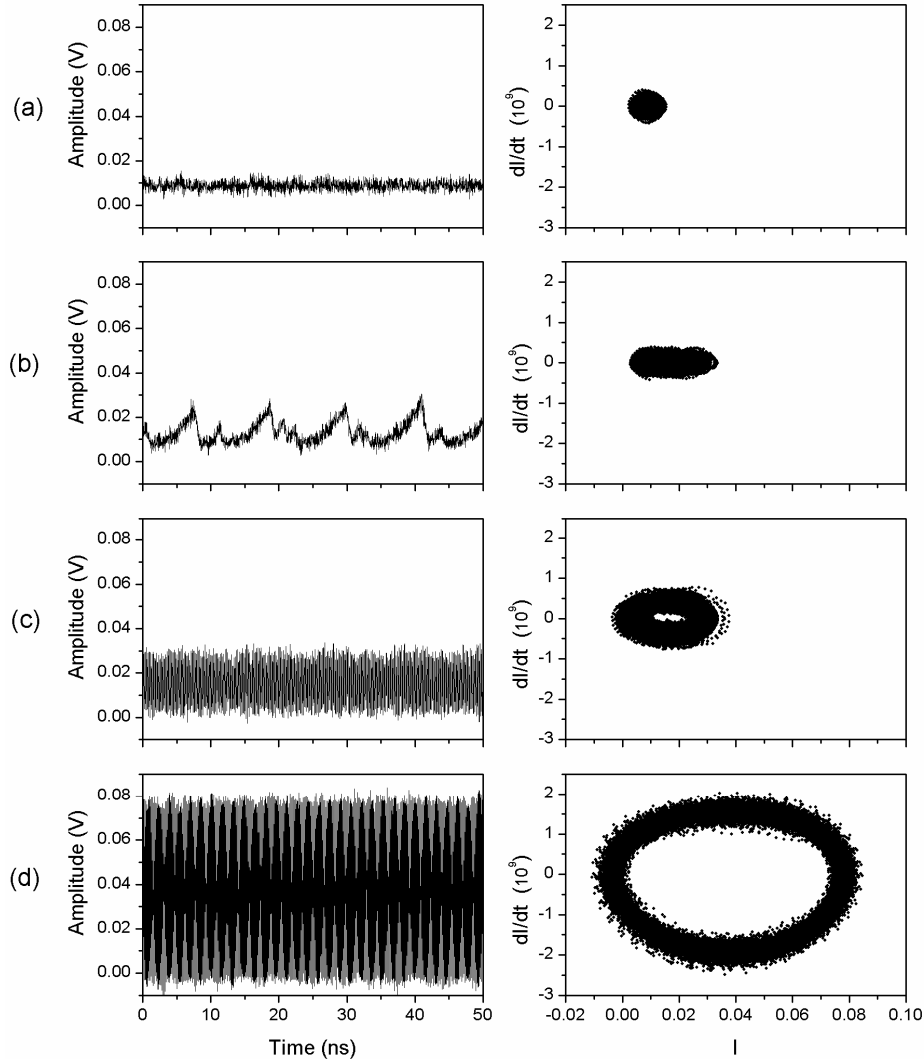


Fig. 9. Sequence of time series (left) and phase portraits (right) showing the orthogonal polarization dynamics as it transitions into the stable P1 region. Frequency detuning $\Delta f = 3.62$ GHz. (a) $K = -14.8$ dB, (b) $K = -14.14$ dB, (c) $K = -10.35$ dB, (d) $K = -2.1$ dB.

The frequency detuning range from 5.36 GHz to 6.86 GHz is characterized by a transition in which a low frequency amplitude modulation of a high frequency oscillation occurs. In

general, increasing the injection strength has the effect of gradually increasing the peak-to-peak amplitude of the orthogonal polarization dynamics, during which the amplitude modulation first appears as a fairly regular envelope (Fig. 10(b)), which then develops into a chaotic modulation (Fig. 10(c)) as the injection strength is increased. Further increase of K pushes the system into the stable P1 region (Fig. 10(e)).

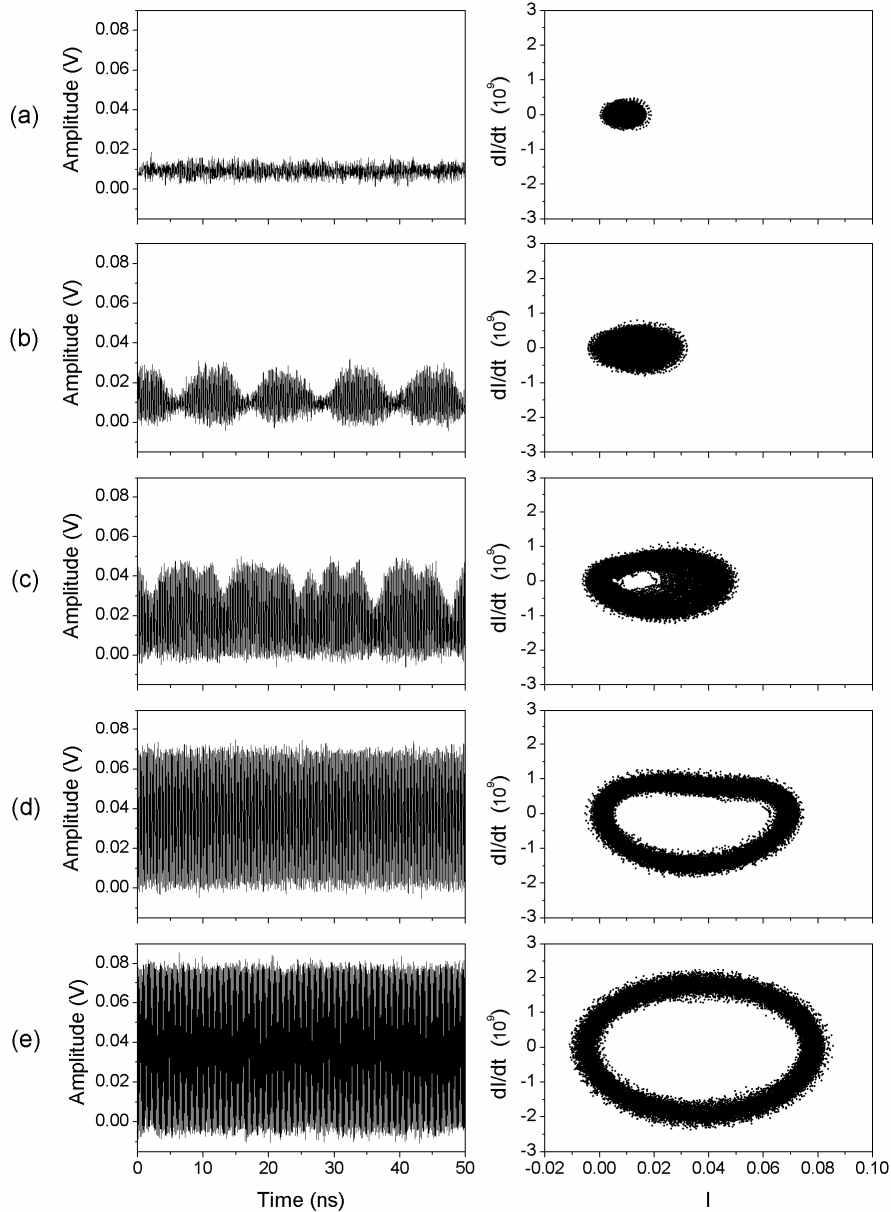


Fig. 10. Sequence of time series (left) and phase portraits (right) showing the orthogonal polarization dynamics as it transitions into the stable P1 region. Frequency detuning $\Delta f = 5.61$ GHz, (a) $K = -10.42$ dB, (b) $K = -9.89$ dB, (c) $K = -8.35$ dB, (d) $K = -7.85$ dB, (e) $K = -2.65$ dB.

For frequency detuning greater than 6.86 GHz, the orthogonal polarization dynamics recorded in this experiment for increasing injection strength showed a rapid transition from

low amplitude noise to fairly robust P1 or P2 oscillations, without any intermediate transitional states.

3.6 Negative frequency detuning

For negative frequency detuning, the area of interest is the isolated region seen at low injection strength and $\Delta f \approx 0$ to -5 GHz. This island is bordered by the injection locked region on one side, and a region of noisy low amplitude dynamics on the other (when the device is lasing on the parallel polarization mode). The transitions to this region are much more dramatic than those generally seen in the case of positive detuning. The system was observed to switch rapidly from ‘no dynamics’ to spiky pulse-like dynamics, such as those time series seen in Figs. 4(b), 4(c) and 4(f). There does not appear to be any systematic variation in the number or frequency of these pulse events in this region. This type of dynamic looks quite similar to pulses resulting from excitability in relation to optically injected semiconductor lasers [37, 38], in quantum dot devices [39], and more recently in comparing quantum well and quantum dot semiconductor lasers [40]. The major difference between this study and those previous works is that they deal with edge-emitting devices rather than the VCSEL device used here. The subject of excitability in VCSELs under polarized optical injection has not yet been addressed theoretically. It is possible there is a similar mechanism at work in this region of the VCSEL parameter space although further investigations, focusing on improved experimental resolution in this region of the parameter space and a thorough theoretical analysis of the VCSEL model, would be required to confirm this interpretation.

Closer inspection of the time series from this region reveals an interesting feature of these random pulsed-like fluctuations, unique to VCSELs. A typical example is shown in Fig. 11.

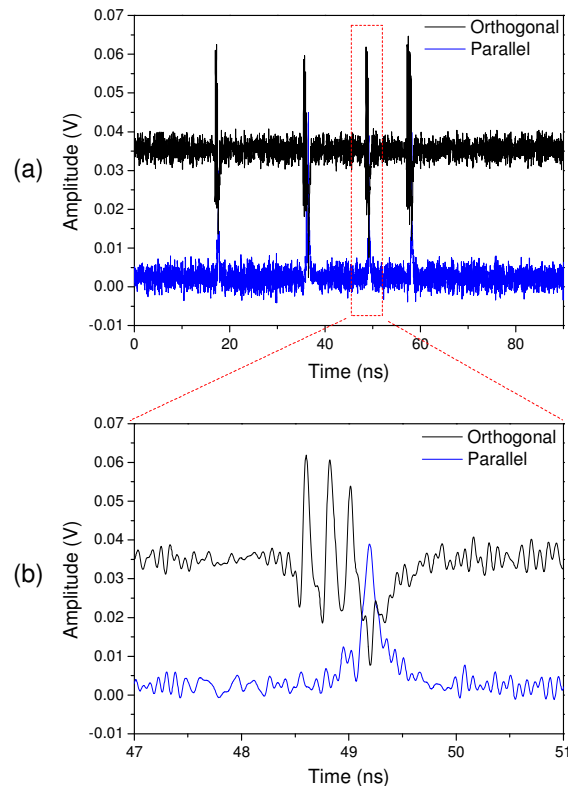


Fig. 11. (a) Time series of both parallel and orthogonal polarizations at $\Delta f = 0.12$ GHz, $K = -14.9$ dB. (b) Region of the time series showing a pre-pulse oscillation event.

Again in this region we see anti-correlated dynamics between the two polarizations. An oscillation with a functional form like a relaxation oscillation has been triggered on the orthogonally polarized light. A build in power in the parallel polarization is seen to begin at about the minimum of the second full cycle of the “orthogonal” oscillation. This can also be interpreted as an oscillation being triggered on the parallel mode light, but this oscillation appears to be more heavily damped. Power recovery to the more favored orthogonal polarization occurs in tandem with damping of the parallel oscillation or pulse. Features of this type are only seen in time series where the laser is operated with very close to zero detuning and low injection strengths. The frequency of the “orthogonal” oscillations appear to increase with the injection strength as shown in Fig. 12, indicating that this is likely an undamping of the VCSEL relaxation oscillation frequency. The relaxation oscillation frequency is known to increase under increased injection [42]. The graph in Fig. 12 shows the frequency of the oscillation approaching the free-running VCSEL relaxation oscillation frequency (approximately 4 GHz) as injection strength is decreased.

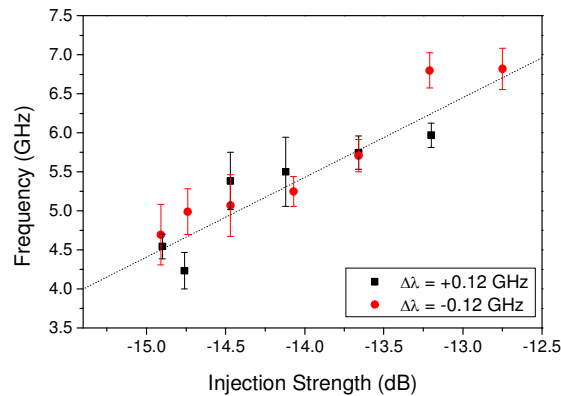


Fig. 12. Frequency of pre-pulse oscillation in the orthogonal polarization for frequency detuning close to zero and low injection strength.

There is some significant variation in the oscillation frequency between events in the same time series as indicated by the error bars in Fig. 12. These represent the standard deviation of the frequencies of each oscillation event. Also contributing to the uncertainty is the fact there may only be a few such oscillation events in each 100 ns time series. There are 4 events in Fig. 11(a) from which the frequency has been measured. This feature of the dynamics would benefit from a follow-up experiment focusing on capturing more data at smaller (K , Δf) intervals.

As the frequency detuning becomes more negative the dynamics become more complicated and look similar to the multipulse excitability seen in other edge-emitting semiconductor laser systems [37–40], albeit with the additional associated polarization mode dynamics. An example of this is shown in Fig. 13.

These pulses are an interesting feature of the dynamics that has come out of this study. Whilst not the focus of this paper they are interesting and comparing them with excitability phenomena seen in other semiconductor laser system is a goal of future work.

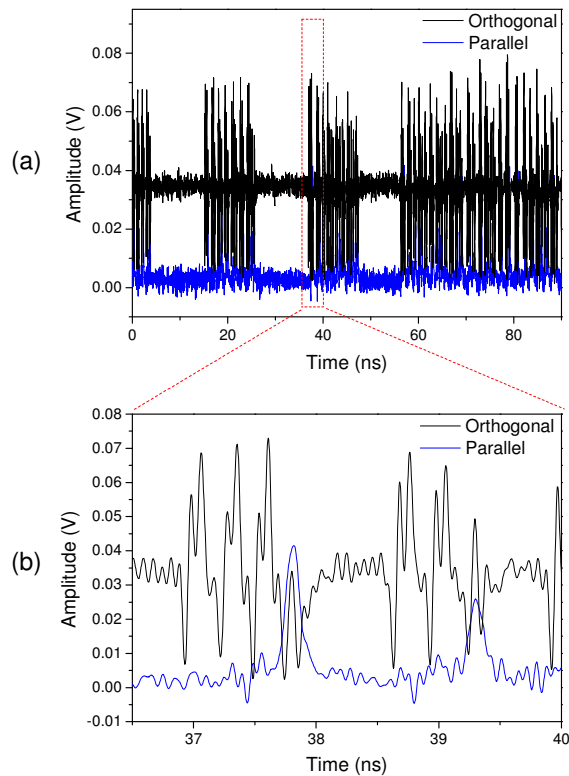


Fig. 13. (a) Time series of both parallel and orthogonal polarizations at $\Delta f = -1.62$ GHz, $K = -9.3$ dB. (b) Region of the time series showing multipulse events.

4. Conclusion

Protocols have been developed to analyze time variation, on sub nanosecond timescales, of the output-power dynamical state of a VCSEL laser subject to optical injection. Using maps of the sub-ns windowed peak-to-peak amplitude standard deviation and/or the standard deviation in time interval between local maxima as a percentage of the average time interval, allows clear identification of regions where the dynamical output changes on these timescales. This in turn facilitates detailed analysis of the evolution of the time dependence of the dynamical state in the regions so identified. In the case of the optically injected VCSEL laser with positive frequency detuning this highlights competition between two polarization modes as mutual damping mechanisms of the dynamic P1 or P2 oscillation. These analysis tools for experimental and simulation data will facilitate identifying regions of the parameter space where increased sensitivity to coupling effects occurs. These regions may be particularly useful in testing theoretical models of the nonlinear dynamical system.

Acknowledgments

This research was supported by the Australian Research Council (Linkage Project LP100100312) and Macquarie University. The work at University of Essex has been funded in part by the UK Engineering and Physical Science Research Council (EPSRC) under project EP/G012458/1 and by the European Commission under the Programme FP7 Marie Curie Intra-European Fellowships Grant PIEF-GA-2008-219682. Agilent UK is acknowledged for the loan of their DSA91304A oscilloscope. We would like to thank anonymous reviewers for helpful comments about alternative interpretations of the observed dynamics.